Structural Studies of Human Histone Deacetylase 8 and Its Site-Specific Variants Complexed with Substrate and Inhibitors[†,‡]

Daniel P. Dowling,[§] Stephanie L. Gantt,[||,⊥] Samuel G. Gattis,[||] Carol A. Fierke,[||] and David W. Christianson*[,§]

Roy and Diana Vagelos Laboratories, Department of Chemistry, University of Pennsylvania, Philadelphia, Pennsylvania 19104-6323, and Departments of Chemistry and Biological Chemistry, University of Michigan, 930 North University Avenue, Ann Arbor, Michigan 48109-1055

Received August 26, 2008; Revised Manuscript Received October 30, 2008

ABSTRACT: Metal-dependent histone deacetylases (HDACs) require Zn^{2+} or Fe^{2+} to regulate the acetylation of lysine residues in histones and other proteins in eukaryotic cells. Isozyme HDAC8 is perhaps the archetypical member of the class I HDAC family and serves as a paradigm for studying structure−function relationships. Here, we report the structures of HDAC8 complexes with trichostatin A and 3-(1-methyl-4-phenylacetyl-1*H*-2-pyrrolyl)-*N*-hydroxy-2-propenamide (APHA) in a new crystal form. The structure of the APHA complex reveals that the hydroxamate C═O group accepts a hydrogen bond from Y306 but does not coordinate to Zn^{2+} with favorable geometry, perhaps due to the constraints of its extended π system. Additionally, since APHA binds to only two of the three protein molecules in the asymmetric unit of this complex, the structure of the third monomer represents the first structure of HDAC8 in the unliganded state. Comparison of unliganded and liganded structures illustrates ligand-induced conformational changes in the L2 loop that likely accompany substrate binding and catalysis. Furthermore, these structures, along with those of the D101N, D101E, D101A, and D101L variants, support the proposal that D101 is critical for the function of the L2 loop. However, amino acid substitutions for D101 can also trigger conformational changes of Y111 and W141 that perturb the substrate binding site. Finally, the structure of H143A HDAC8 complexed with an intact acetylated tetrapeptide substrate molecule confirms the importance of D101 for substrate binding and reveals how Y306 and the active site zinc ion together bind and activate the scissile amide linkage of acetyllysine.

Important biological processes are often regulated by the reversible covalent modification of proteins involved in transcriptional regulation or signaling pathways (*1*−*3*). For example, the N-termini of eukaryotic histone proteins are subject to various covalent chemical modifications such as acetylation, phosphorylation, methylation, ubiquitination, and ADP-ribosylation, and these modifications influence transcriptional activation (*1, 4*). Consider the acetylation of lysine residues as catalyzed by histone acetyltransferases. This particular chemical modification plays an important role in the regulation of chromatin remodeling, gene transcription, and cellular proliferation, and increased levels of histone acetylation generally correlate with increased transcriptional activity (*5*−*8*). The chemical modification is reversed by histone deacetylases, which function to maintain a dynamic balance in the acetylation levels of protein targets (*7, 9*).

Phylogenic analyses reveal four distinct classes of human histone deacetylases: class I (HDAC[1] enzymes 1−3 and HDAC8), class II (HDAC enzymes 4−7, HDAC9, and HDAC10), class III (NAD-dependent human sirtuins 1−7), and class IV (HDAC11) (*2, 10*). These enzymes are implicated in a wide variety of biological processes such as apoptosis, differentiation, proliferation, and senescence (*11*). However, questions remain regarding the precise cellular location(s), substrate(s), and function(s) of certain deacetylases (*12*). For example, in addition to a role in covalent histone modification in the nucleus (*13*), HDAC8 is also implicated in protecting a telomerase activator, the human ever-shorter telomeres 1B protein, from ubiquitin-mediated degradation (*14*). Additionally, HDAC8 is found in the cytosol of differentiating smooth muscle cells, where it associates with the α-actin cytoskeleton and plays a potential role in regulating smooth muscle contractility (*15*). Interestingly, recent studies indicate that a potent HDAC8 inhibitor

[†] This work was supported by the National Institutes of Health Grants GM49758 (D.W.C.) and GM40602 (C.A.F.).

[‡] The atomic coordinates of HDAC8 complexed with TSA and APHA, D101 HDAC8 variants complexed with M344, and H143A HDAC8 complexed with a tetrapeptide substrate have been deposited in the Protein Data Bank (www.rcsb.org) with accession codes 3F0R, 3F07, 3EW8, 3EZT, 3EZP, 3F06, and 3EWF, respectively.

* To whom correspondence should be addressed. Tel: 215-898-5714. Fax: 215-573-2201. E-mail: chris@sas.upenn.edu.

[§] University of Pennsylvania.

[||] University of Michigan.

[⊥] Current address: Department of Biochemistry, University of Illinois, Urbana−Champaign, IL 61801.

[1] Abbreviations: ADP, adenosine diphosphate; APHA, 3-(1-methyl-4-phenylacetyl-1*H*-2-pyrrolyl)-*N*-hydroxy-2-propenamide; BME, β-mercaptoethanol; CRA-A, 5-(4-methylbenzoylamino)biphenyl-3,4′-dicarboxylic acid 3-dimethylamide 4′-hydroxyamide; HDAC, histone deacetylase; HDLP, histone deacetylase-like protein; M344, 4-(dimethylamino)-*N*-[7-(hydroxyamino)-7-oxoheptyl]benzamide; MES, 2-(*N*-morpholino)ethanesulfonic acid; NAD, nicotinamide adenine dinucleotide; NCS, noncrystallographic symmetry; SAHA, suberoylanilide hydroxamic acid; TCEP, tris(2-carboxyethyl)phosphine hydrochloride; TSA, trichostatin A.

10.1021/bi801610c CCC: $40.75
Published on Web 11/24/2008

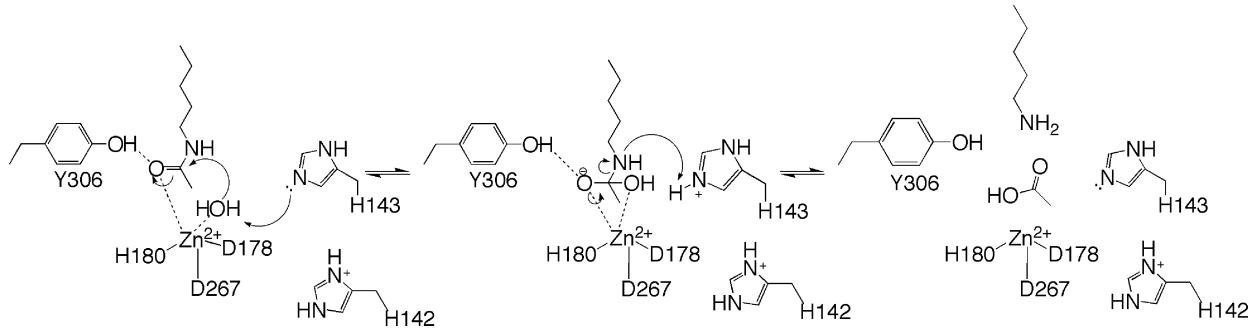

FIGURE 1: Proposed mechanism of histone deacetylase 8 (HDAC8) (*17*−*19, 23*−*25*).

does not increase histone or tubulin acetylation levels; yet, this inhibitor induces apoptosis in T cell-derived tumor cells (*16*). Other histone deacetylases also have non-histone protein substrates that regulate various biological functions, e.g., p53 (HDAC1 substrate) and signal transducers of TGF-β (Smad7) and cytokines (Stat3) (HDAC1 and HDAC3 substrates) (*12*). Thus, the designation "histone deacetylase" is somewhat limited in that it does not adequately represent the various cellular locations and diverse biological functions served by this enzyme family.

Crystal structures of HDAC8 (*17, 18*) and histone deacetylase-like protein (HDLP) from *Aquifex aeolicus* (*19*) unexpectedly revealed a protein fold topologically identical to that of the unique α/β fold first observed in rat liver arginase, a binuclear manganese metalloenzyme (*20*). This structural homology was quite surprising given that these enzymes are related by insignificant (~14%) amino acid sequence identity. However, in contrast with arginase, the crystal structures of HDAC8 and HDLP reveal the binding of a single metal ion interpreted as Zn^{2+} to a site corresponding to $Mn^{2+}{}_B$ of arginase (*21, 22*). Thus, the metal ion specificity and stoichiometry of arginase and the metal-dependent histone deacetylases have substantially diverged in evolution (*22*). Curiously, recombinant HDAC8 activity (k_{cat}/K_M) is 9.4-fold and 2.8-fold higher with Co^{2+} and Fe^{2+}, and 20-fold lower with Mn^{2+}, in comparison with Zn^{2+}, respectively (*23*), leaving unanswered questions regarding the metal ion specificity of HDAC8 *in vivo*.

The chemical mechanism proposed for metal-dependent histone deacetylases is based on biochemical and structural studies of HDLP (*19*) and HDAC8 (*17, 18, 23*−*25*) (Figure 1). In the first step of catalysis, the active site metal ion and a histidine residue promote the attack of a nucleophilic metal-bound water molecule at the scissile carbonyl group of acetyllysine, which is polarized by coordination to Zn^{2+} and a hydrogen bond with Y306 (*17*−*19, 25*−*27*). This metal-bound water molecule is within hydrogen-bonding distance to both H142 and H143 (*25, 26*), and either H142 or H143 could potentially be the general base. The hydroxyl group of Y306 is also positioned to stabilize the oxyanion of the resulting tetrahedral intermediate, the collapse of which is proposed to be facilitated by proton transfer from H143 to the leaving amino group of lysine (*20*).

The active site metal ion is critical for the molecular recognition of inhibitors by histone deacetylases. Hydroxamic acid derivatives such as trichostatin A (TSA), suberoylanilide hydroxamic acid (SAHA), 4-(dimethylamino)-*N*-[7-(hydroxyamino)-7-oxoheptyl]benzamide (M344), and 3-(1-methyl-4-phenylacetyl-1*H*-2-pyrrolyl)-*N*-hydroxy-2-propenamide (APHA) (Figure 2) exhibit IC_{50} values in the micromolar to nanomolar range (*12*). Crystal structures of HDAC8 complexed with these compounds show that the hydroxamic acid moiety of each inhibitor chelates the active site zinc ion while the aliphatic linker of each inhibitor makes numerous interactions in the active site tunnel (*17, 18*). These structural features are believed to account for the high affinity and resultant antitumor effects of these inhibitors (*2, 12*). Thus, the structures of histone deacetylase−inhibitor complexes promise to illuminate aspects of mechanism and affinity that may guide the design of potential cancer chemotherapeutic agents.

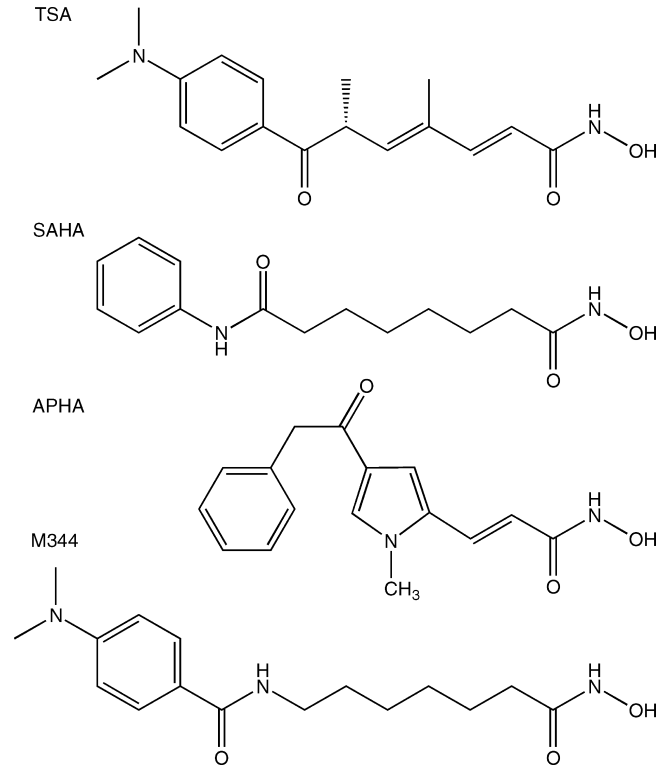

FIGURE 2: Molecular structures of trichostatin A (TSA), suberoylanilide hydroxamic acid (SAHA), 3-(1-methyl-4-phenylacetyl-1*H*-2-pyrrolyl)-*N*-hydroxy-2-propenamide (APHA), and 4-(dimethylamino)-*N*-[7-(hydroxyamino)-7-oxoheptyl]benzamide (M344).

Here, we report the X-ray crystal structures of human HDAC8 complexed with the inhibitors TSA and APHA in a new crystal form. Interestingly, since APHA binds to only two of the three protein molecules in the asymmetric unit, the structure of the third monomer provides a view of unliganded HDAC8. Comparison of unliganded and liganded structures illustrates ligand-induced conformational changes in the L2 loop that likely accompany substrate binding and

catalysis. Furthermore, these structures, along with those of the D101N, D101E, D101A, and D101L variants, confirm that the strictly conserved side chain of D101 is crucial for the function of the L2 loop. However, amino acid substitutions for D101 can also trigger conformational changes of Y111 and W141 that perturb the substrate binding site. Finally, the structure of H143A HDAC8 complexed with an intact acetylated tetrapeptide substrate molecule further illustrates the role of D101 in substrate binding and reveals how Y306 and the active site zinc ion together bind and activate the amide carbonyl group of the substrate.

MATERIALS AND METHODS

Human HDAC8 Plasmid Construct. The pET-20b-derived HDAC8-His expression plasmid with optimized codon usage, pHD2-His (*23*), was modified to add a factor Xa cleavage site between the sequence encoding human HDAC8 and the C-terminal His_6 tag, generating the plasmid pHD2-Xa-His. The amino acid sequence encoded by this construct was identical to that reported by Vannini and colleagues (*18*). Overlap extension of primers 1 and 2 was used to generate a DNA insert containing the *Stu*I and *Sac*II restriction sites that encoded the HDAC8 sequence from Arg353 onward, the factor Xa cleavage site (IEGR|GS), and the His_6 tag (primer 1, 5′-GCT TTG TTA G*CC GCG G*GA TCT CAG TGG TGG TGG TGG TGG TGA GAA CCA CGA CCT TCG ATA ACA A<u>CG TGT TTC AGG TTG CCT TTG</u>-3′; primer 2, 5′-GCC AAG CTG C*AG GCC T*GA CCG CAA CGA GCC GCA CCG CAT CCA GCA GAT CCT CAA CTA CAT CAA AGG <u>CAA CCT GAA ACA CGT TG</u>-3′; restriction sites are indicated by italics, and the overlapping regions are underlined) (*23*). This insert was amplified by the polymerase chain reaction using primers 3 and 4 (primer 3, 5′-GCC AAG CTG CAG GCC TGA C-3′; primer 4, 5′-GCT TTG TTA GCC GCG GGA TC-3′). Using a QuikChange site-directed mutagenesis kit (Stratagene), a *Stu*I restriction site was introduced into pHD2-His at Arg353, and a *Sac*II restriction site was added five nucleotides after the stop codon following the His_6 tag. This modified plasmid and the DNA insert were each digested with *Stu*I and *Sac*II and then purified using agarose gel electrophoresis. Finally, the insert and the plasmid were combined using T4 DNA ligase (New England Biolabs) to generate the plasmid pHD2-Xa-His.

Five mutants were generated using the QuikChange mutagenesis kit (Stratagene) with primers 1 and 2 for each respective mutant with the pHD2-Xa-His template as follows: D101E, primer 1, 5′-GCT AGG TTA Tga aTG CCC AGC CAC-3′, primer 2, 5′-GTG GCT GGG CAt tcA TAA CCT AGC-3′; D101N, primer 1, 5′-GCT AGG TTA Taa cTG CCC AGC CAC-3′, primer 2, 5′-GTG GCT GGG CAg ttA TAA CCT AGC-3′; D101L, primer 1, 5′-GCT AGG TTA Tct gTG CCC AGC CAC-3′, primer 2, 5′-GTG GCT GGG CAc agA TAA CCT AGC-3′; D101A, primer 1, 5′-GCT AGG TTA Tgc cTG CCC AGC CAC-3′, primer 2, 5′-GTG GCT GGG CAg gcA TAA CCT AGC-3′; H143A, primer 1, 5′-GGT CTG GAG GGT GGC ATg cTG CAA AGA AAG ATG AAG C-3′, primer 2, 5′-GCT TCA TCT TTC TTT GCA gcA TGC CAC CCT CCA GAC C-3′. PCR products were transformed into XL1-Blue cells for DNA isolation and sequencing.

Purification of Human HDAC8. Protein was expressed in *Escherichia coli* BL21(DE3) cells and purified as described (*18*) with slight modifications. Briefly, cells were harvested and lysed in 50 mM Tris (pH 8.0), 5% glycerol, 0.25% (w/v) 1-*O*-*n*-octyl-β-D-glucopyranoside, 1 mM β-mercaptoethanol (BME), 10 μg/mL phenylmethanesulfonyl fluoride, and 1 μg/mL N_α-*p*-tosyl-L-arginine methyl ester hydrochloride. The soluble portion of the lysate was loaded onto either nickel nitrilotriacetic acid or TALON affinity resin (preequilibrated with 50 mM Tris (pH 8.0), 500 mM KCl, 5% glycerol, 10 mM imidazole, and 1 mM BME) and eluted with two steps of 50 and 250 mM imidazole. Protein fractions were pooled, dialyzed into the same buffer with no salt, and loaded onto a GE HiTrap Q HP column. Protein was eluted with a stepwise gradient from 0 to 500 mM KCl, and protein fractions were then concentrated to <5 mL and loaded onto a Superdex 26/60 Amersham column preequilibrated in Superdex buffer (50 mM Tris (pH 8.0), 150 mM KCl, 5% glycerol, and 1 mM dithiothreitol) to yield >95% pure protein.

Metal-free HDAC8 was prepared as previously described (*23*). All plastics were presoaked in 1 mM EDTA followed by thorough rinsing with Milli-Q ddH_2O. All pipet tips and sample tubes were certified trace metal free. For Co^{2+}-HDAC8 activity measurements, metal-free protein was incubated on ice with equimolar Co^{2+} (Aldrich, 99.998% trace metals basis).

Activity measurements for HDAC8 variants were performed as previously described for the wild-type enzyme (*23*) using the commercially available Fluor de Lys kit (BIOMOL) with Fluor de Lys HDAC8 substrate. Because of the increased catalytic efficiency of Co^{2+}-HDAC8 in comparison with Zn^{2+}-HDAC8 (*23*), Co^{2+}-substituted D101 and H143 variants were prepared to ensure the measurement of residual catalytic activity. Accordingly, HDAC8 variants that were inactive with Co^{2+} were also inactive with Zn^{2+}. Assays of catalytically active variants were performed in triplicate or quadruplicate. The IC_{50} assay mixture used to study HDAC8−APHA complexation contained 50 μM fluorogenic peptide substrate, 0.5 μM HDAC8, 25 mM Tris (pH 8.0), 137 mM NaCl, 2.7 mM KCl, 1 mM $MgCl_2$, and 0.1−100 μM APHA. Reactions were incubated at 37 °C for 30 min, quenched with stop solution (Developer II (BIOMOL) and 1 μM TSA), and tested for deacetylated product using a fluorescence plate reader (Fluoroskan II) (ex = 355 nm, em = 460 nm).

Crystal Structure Determinations of Human HDAC8 Variants and Inhibitor Complexes. The Zn^{2+}-HDAC8 variants were used for crystallographic studies. A new crystal form of HDAC8 was discovered for the HDAC8−TSA and HDAC8−APHA complexes using minor modifications of previously published conditions (*18*). The inhibitors TSA and APHA were purchased from Sigma and used without further purification. Briefly, a 4 μL hanging drop of 5 mg/mL HDAC8 in 50 mM Tris (pH 8.0), 150 mM KCl, 5% glycerol, 1 mM dithiothreitol, and 2 mM inhibitor was mixed with a 4 μL drop of precipitant buffer (0.1 M 2-(*N*-morpholino)-ethanesulfonic acid (MES) (pH 5.3), 1−5% polyethylene glycol (PEG) 6000, 2 mM tris(2-carboxyethyl)phosphine (TCEP)) and a 0.4 μL drop of 0.3 M Gly-Gly-Gly and was equilibrated against a 600 μL reservoir of precipitant buffer at room temperature. The final pH in the crystallization drop

Table 1: Data Collection and Refinement Statistics

structure	wild-type HDAC8−TSA complex	wild-type HDAC8−APHA complex	D101E HDAC8−M344 complex	D101A HDAC8−M344 complex	D101L HDAC8−M344 complex	D101N HDAC8−M344 complex	H143A HDAC8−substrate complex
(A) Unit Cell							
space group	$P2_1$	$P2_1$	$P2_1$	$P2_1$	$P2_12_12$	$P2_1$	$P2_12_12_1$
unit cell parameters							
a,*b*,*c* (Å)	87.9, 90.7, 92.1	88.4, 90.4, 92.8	53.5, 84.7, 94.7	56.0, 85.9, 94.8	90.6, 88.9, 52.4	55.3, 85.9, 94.6	82.9, 91.8, 196.6
α, *β*, *γ* (deg)	90, 94.6, 90	90, 94.7, 90	90, 98.1, 90	90, 93.7, 90	90, 90, 90	90, 93.6, 90	90, 90, 90
(B) Data Collection							
resolution limits (Å)	50−2.54	32−3.3	50−2.85	50−2.55	50−1.8	50−2.65	50−2.5
total/unique reflections	86137/45639	40230/21912	67864/19641	53446/28356	74694/39760	48874/25531	99678/52790
completeness (%) (overall/outer shell)	96.8/97.4	98.8/99.5	99.6/99.5	98.2/92.4	99.7/99.5	99.6/96.8	99.4/95.2
R_{merge}[a] (overall/outer shell)	0.097/0.508	0.136/0.435	0.112/0.437	0.099/0.302	0.089/0.535	0.14/0.505	0.137/.517
$I/\sigma(I)$ (overall/outer shell)	11.7/2.3	8.0/3.2	10.7/2.4	8.2/4.1	20/3.9	10.2/1.9	11.8/1.8
no. of reflections (work set/test set)	40864/2177	20014/828	18854/771	25224/1875	38536/2319	20618/1045	45347/4032
(C) Refinement							
R/R_{free}[b]	0.210/0.256	0.216/0.260	0.225/0.257	0.229/0.258	0.175/0.201	0.225/0.262	0.199/0.229
protein atoms[c]	8466	8383	5594	5568	2785	5588	11340
water molecules[c]	102	14	14	30	252	37	299
ligand atoms[c]	132	42[d]	44	44	22	44	244
metal ions[c]	9	9	6	6	3	6	14
glycerol atoms[c]					6		
reduced BME atoms[c,e]			8	8	4	8	
rmsd bond lengths (Å)	0.007	0.008	0.007	0.008	0.008	0.008	0.007
rmsd bond angles (deg)	1.3	1.3	1.3	1.3	1.4	1.3	1.3
rmsd dihedral angles (deg)	22.0	22.0	22.1	22.3	22.5	23.1	22.7
rmsd improper dihedral angles (deg)	0.8	0.8	0.8	0.8	1.0	0.9	0.8

[a] $R_{merge} = \sum|I - \langle I\rangle|/\sum|\langle I\rangle|$, where I is the observed intensity and $\langle I\rangle$ is the average intensity calculated for replicate data. [b] Crystallographic R factor, $R = \sum(|F_o| - |F_c|)/\sum|F_o|$, for reflections contained in the working set. Free R factor, $R_{free} = \sum(|F_o| - |F_c|)/\sum|F_o|$, for reflections contained in the test set excluded from refinement. $|F_o|$ and $|F_c|$ are the observed and calculated structure factor amplitudes, respectively. [c] Per asymmetric unit. [d] Refined APHA occupancy = 0.7. [e] Refined BME molecules with occupancies between 0.5 and 0.8.

was 5.8. Large plate-like crystals appeared within 1−5 days and grew to typical dimensions of 300 × 150 × 50 μm^3. Crystals were harvested and cryoprotected in 25 mM Tris-HCl, 50 mM MES (pH 5.8), 75 mM KCl, 0.5 mM TCEP, 50 μM inhibitor, and 8% or 20% polyethylene glycol (PEG) 6000 for the APHA and TSA complexes, respectively, or 10% or 30% glycerol for the TSA and APHA complexes, respectively.

The D101 HDAC8 variants were similarly crystallized and cryoprotected with slight modification of the precipitant buffer solution. Specifically, the D101A, D101L, D101N, and D101E variants complexed with M344 (purchased from Sigma) crystallized with 1−5% PEG 6000, PEG monomethyl ether 550, PEG 35000, and PEG dimethyl ether 2000, respectively. Crystals were cryoprotected in the same buffer with a final glycerol concentration of 30% and 50 μM inhibitor. The H143A variant complexed with an acetylated tetrapeptide substrate (*N*-acetyl-arginine-histidine-acetyl-lysine-acetyllysine-coumarin) was crystallized using a precipitant buffer of 50 mM Tris-HCl (pH 8.0), 50 mM $MgCl_2$, 150 mM KCl, 13% PEG 6000, 2 mM TCEP, and 3.2 mM substrate. Crystals were subsequently transferred to a cryoprotectant buffer of 50 mM Tris-HCl (pH 8.0), 25 mM $MgCl_2$, 75 mM KCl, 20% PEG 6000, 1 mM TCEP, 20% glycerol, and 50 μM substrate as described previously for Y306F HDAC8 (*25*).

Diffraction data were measured on beamline F1 at the Cornell High Energy Synchrotron Source (CHESS, Ithaca, NY) for crystals of the HDAC8−TSA complex and beamlines XL12-B and X29 at the Brookhaven National Synchrotron Light Source (NSLS, Brookhaven, NY) for crystals of the HDAC8−APHA and D101E HDAC8 variant−M344 complexes. Diffraction data for the remaining D101 HDAC8 variant−M344 complexes and the H143A HDAC8−substrate complex were collected at beamlines ID-24C/E at the Advanced Photon Source, Northeastern Collaborative Access Team (APS, NECAT, Argonne, IL). Crystal and data collection statistics are recorded in Table 1.

Data were indexed and merged using HKL2000 (*28*) and MOSFLM (*29*). Molecular replacement calculations were performed with AMoRe (*30*) using the atomic coordinates of an inhibited form of HDAC8 less inhibitor and solvent atoms (PDB accession code 1W22) (*18*) as a search probe for rotation and translation functions for the HDAC8−TSA complex. This refined solution was used for molecular replacement with the HDAC8−APHA complex. Similarly, molecular replacement calculations for the D101 HDAC8 variant−M344 complexes and the H143A HDAC8−substrate complex were performed with AMoRe (*30*) or PHASER (*31*) using the structure of wild-type HDAC8 minus ligand and solvent atoms as a search probe (PDB accession codes 1T67 and 2V5W, respectively) (*17, 25*). Iterative cycles of refinement and model building were performed using CNS (*32*) and O (*33*), respectively, in order to improve each structure as guided by R_{free} values. Strict noncrystallographic symmetry (NCS) restraints were initially used during the first few cycles of refinement of each complex and relaxed into appropriately weighted restraints early in refinement. In the HDAC8−TSA and HDAC8−APHA complexes, residues M1−Q12 at the N-termini of all monomers, residues A32−K33 of monomer A, and residues G86−E95 of monomer C of the HDAC8−TSA complex appeared to be disordered and were excluded from the final model. For the HDAC8−APHA complex, residues Q84−E106 of monomer C appeared to be disordered and were excluded from the final model (APHA was not observed to bind to monomer

C). For the HDAC8-D101 variants complexed with M344, disordered regions correspond to those previously identified for the wild-type enzyme (*17*). Finally, residues M1−S13 in all monomers of the H143A HDAC8−substrate complex are disordered and excluded from the final model. All refinement statistics are recorded in Table 1.

RESULTS AND DISCUSSION

Including the three new crystal forms described herein, a total of nine different crystal forms have been observed for HDAC8, its variants, and its inhibitor complexes (*17, 18, 25*). Regardless of the crystal form, the enzyme contains a single Zn^{2+} ion bound in its active site (Zn^{2+}:protein ratio = 1:1.2 based on inductively coupled plasma measurements); additionally, two K^+ ions bind to structural sites identified in earlier studies (*17, 18*). Inhibitor binding in these complexes affects the conformations of loop segments L1 (S30−P35) and L2 (E85−E106) (*17, 18*), which in turn appear to affect the packing of HDAC8 monomers in the crystal lattice. Conformational variability of the L1 and L2 loop segments may account for the polymorphism observed for HDAC8−inhibitor complexes.

Except for the structure of the H143A HDAC8−substrate complex determined at pH 8.0, the structures of wild-type and D101 variant HDAC8−inhibitor complexes have been determined at pH 5.8. Given that HDAC8 exhibits a bell-shaped pH−rate profile with a low-pH pK_a of ~7, enzyme activity at pH 5.8 is low (*34*). However, the structure of HDAC8 determined at pH 5.8 is generally identical to structures determined at pH values of 6.8−8.0 (*17, 18, 25*), including the structure of the H143A HDAC8−substrate complex determined at pH 8.0 reported herein.

Wild-Type HDAC8−Inhibitor Complexes. The inhibitor APHA (Figure 2) binds to HDAC8 with $IC_{50} = 2.9 \pm 0.6$ μM (data not shown). This compares with IC_{50} values of 0.1 and 0.5 μM measured against maize HD2 and murine HDAC1, respectively (*35*), and an IC_{50} value of 5.9 μM for chloro-substituted APHA against HDAC8 (*36*). The HDAC8−APHA complex is monomeric in the new monoclinic crystal form, and crystal packing is such that monomers A and B form two-dimensional sheets parallel to the *bc* plane, with monomer C connecting adjacent sheets (Figure 3). A second Zn^{2+} binding site is observed in the L2 loop of monomer A, where the metal ion is coordinated by H78, D87, H90, and D92 with approximate tetrahedral coordination geometry (Figure 5). The identity of this metal ion as Zn^{2+} is confirmed in a Bijvoet difference Fourier map calculated with anomalous scattering data (data not shown).

Only one APHA molecule binds to each of monomers A and B (Figure 4), and no inhibitor molecule binds to monomer C. The hydroxamate moiety of APHA does not appear to make a favorable coordination interaction with the active site Zn^{2+} ion. Although the structure is determined at 3.3 Å resolution and is therefore subject to some ambiguity, the inhibitor molecule has limited flexibility due to its extended π system which may impose restraints on its binding conformation. The best interpretation of the electron density map places both oxygens of the hydroxamate moiety ~2.4 Å from the Zn^{2+} ion but poorly oriented for metal coordination.

The hydroxamate C═O group of APHA accepts a hydrogen bond from Y306, and the hydroxamate NH and OH groups make hydrogen bond interactions with H142, H143, and D178 (Figure 4). Insofar as the hydroxamate C═O resembles the carbonyl of an acetyllysine substrate, this binding mode is consistent with the proposed role of Y306 in assisting Zn^{2+} with the activation of the acetyllysine C═O group for nucleophilic attack by a metal-bound solvent molecule promoted by H142 or H143 (Figure 1), as previously proposed by Somoza and colleagues (*17*). The role of both Y306 and Zn^{2+} in substrate activation is consistent with the lack of measurable catalytic activity for Y306F HDAC8 (*25*) as well as the ~7-fold variation in K_M with Zn^{2+}-, Fe^{2+}-, and Co^{2+}-substituted HDAC8 (presuming that K_M reflects enzyme−substrate affinity in the Michaelis complex (*23*)). Notably, the presence of a hydrogen bond donor to assist the active site Zn^{2+} ion in polarizing a substrate C═O moiety was first proposed in the catalytic mechanisms of the prototypical zinc hydrolases thermolysin (*37*) and carboxypeptidase A (*38*).

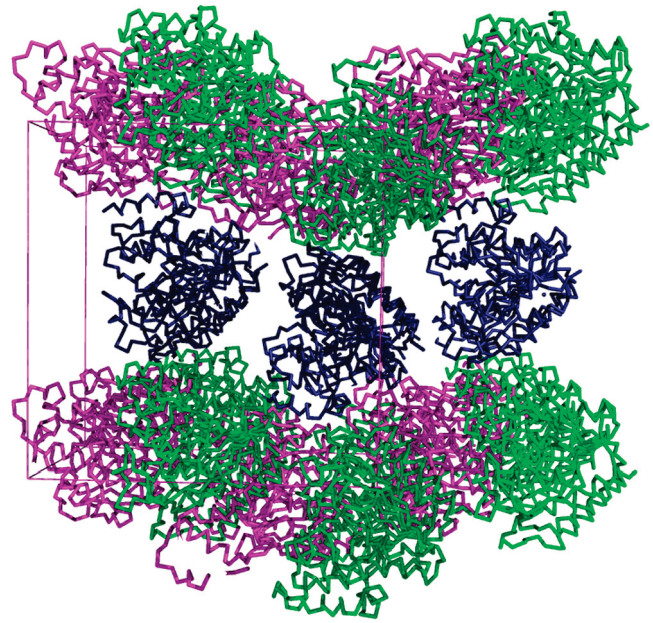

FIGURE 3: Packing of HDAC8 molecules in the new monoclinic crystal form. Monomers A, B, and C appear as pink, green, and dark blue, respectively. The unit cell is depicted in pink (a = 87.90 Å, b = 90.71 Å, c = 92.14 Å, β = 94.6°).

Apart from hydrogen bond interactions with the hydroxamate group, no other polar interactions are observed between HDAC8 and APHA except for an interaction between the carbonyl group adjacent to the pyrrole ring of APHA and the side chain of D101 (Figure 4). Presumably, D101 is protonated in order to accommodate this interaction.

Due to the packing arrangement of HDAC8 in the new monoclinic crystal form (Figure 3), the active site of monomer C is unliganded and therefore represents the first structure of unliganded HDAC8. An electron density peak is observed that may correspond to a nonprotein Zn^{2+} ligand and is interpreted as a solvent molecule. The absence of bound inhibitor appears to be a consequence of the fact that monomer C is much more solvent exposed, which results in increased flexibility for loop L2 (Q84−E106) in this monomer compared with monomers A and B. Loop L2 is disordered in the unliganded enzyme but becomes ordered upon the binding of APHA (Figure 5). With APHA being a lower affinity inhibitor in comparison with TSA, it is

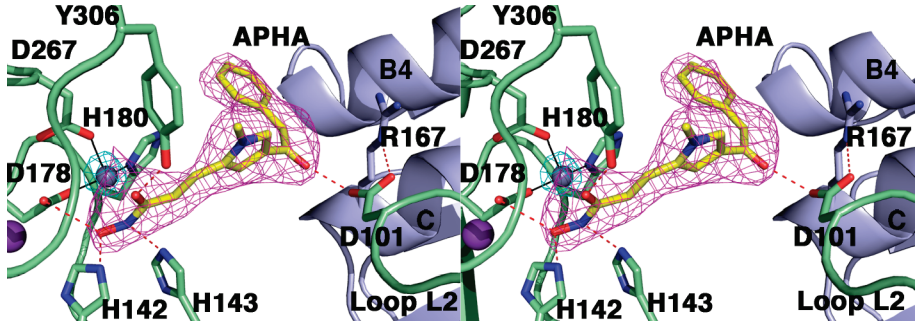

FIGURE 4: Simulated annealing omit map of APHA (magenta, contoured at 3.5σ) and Zn^{2+} (cyan, contoured at 11σ) in monomer B of the HDAC8−APHA complex. α-Helices B4 and C (which contains R167) of monomer C are shown in light blue. The side chain of D101 in the L2 loop of monomer B accepts hydrogen bonds from the pyrrole C═O group of APHA and R167 in helix C of monomer C. Metal coordination and hydrogen bond interactions are shown as solid black and dotted red lines, respectively.

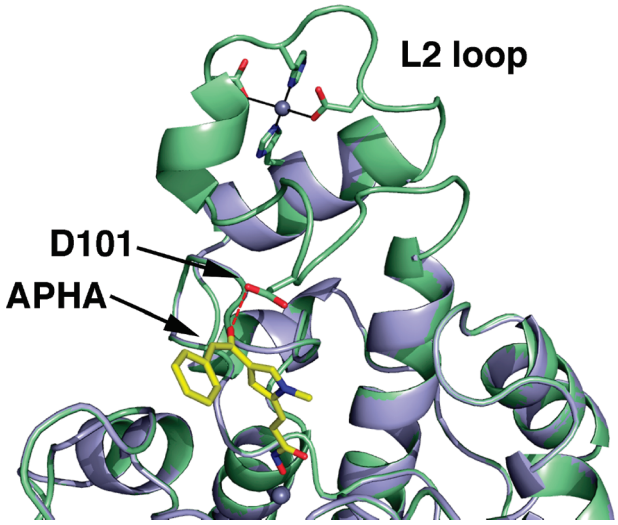

FIGURE 5: Superposition of unliganded monomer C (light blue) and APHA-complexed monomer A (light green) of HDAC8 (Zn^{2+} is gray). Inhibitor binding results in the ordering of the L2 loop, which appears to be mediated by an enzyme−inhibitor hydrogen bond with D101 (red dotted line, also illustrated in Figure 4). A second zinc binding site is observed in the ordered L2 loop of monomer A only. Zn^{2+}_B (gray sphere) interacts with H78 (2.2 Å), D87 (2.6 Å), H90 (2.0 Å), and D92 (2.6 Å).

conceivable that the free energy gain from HDAC8−APHA complexation is insufficient to overcome the free energy cost of L2 loop ordering. In monomer A, loop L2 is buttressed by interactions with α-helices B4 and C of monomer B, and similar interactions occur between monomers B and C (Figure 4).

Finally, the X-ray crystal structure determination of the HDAC8−TSA complex reveals that the tertiary structure of each monomer resembles that previously observed in the tetragonal crystal form (*17*). However, this complex crystallizes as a monomer in the new monoclinic crystal form, in contrast with the dimers observed in other crystal forms where the active site loops and the inhibitors themselves provide extensive surface contact (~1300 Å^2) defining a binary symmetry axis (*17, 18*). Two molecules of TSA bind to monomers A, B, and C, and each makes interactions with the protein that are identical to those previously observed in the tetragonal crystal form (data not shown) (*18*).

D101A, D101L, D101N, and D101E HDAC8 Variants. Interestingly, the carboxylate side chain of D101 is the only strictly conserved residue in the L2 loop in class I and II HDAC enzymes, and this residue is important for substrate and inhibitor binding. Specifically, the side chain of D101 makes critical hydrogen bond interactions with two substrate NH groups (*25*) or the C═O, S═O, or NH groups of certain inhibitors (*17, 18, 25*), including the pyrrole C═O group of APHA (Figure 4). Hydrogen bond interactions between D101 and inhibitor C═O or S═O groups require the protonated carboxylic acid form of D101. Recent crystal structures of human HDAC4 and HDAC7 similarly confirm a key role for the corresponding aspartate residues in their respective L2 loops (*26, 39*), and these aspartate residues are also strictly conserved in histone deacetylase-like amidohydrolases (*27, 40*). That D101A HDAC8 is catalytically inactive confirms that D101 is important for substrate recognition (*25*). However, our studies now demonstrate that D101 is functionally important not only due to its direct interaction with ligands bound in the enzyme active site but also due to its influence on the conformations of other active site residues important for substrate binding, as described below.

Table 2: Catalytic Activity of HDAC8 Variants

variant[a]	k_{cat} (s^{-1})	K_M (μM)	k_{cat}/K_M (M^{-1} s^{-1})	relative rate[b]
Co^{2+}-wild type[c]	1.2 ± 0.2	160 ± 6	7500 ± 300	1.0
Zn^{2+}-wild type[c]	0.90 ± 0.03	1100 ± 50	800 ± 50	0.1
Co^{2+}-D101E	0.15 ± 0.01	140 ± 30	1100 ± 200	0.15
Co^{2+}-D101N	nd[d]	>1000[d]	0.23 ± 0.05	3×10^{-5}
Co^{2+}-D101A[e]	nd[d]	>1000[d]	0.23 ± 0.01	3×10^{-5}
Co^{2+}-D101L	nd[d]	>1000[d]	nd[f]	
Co^{2+}-H143A	nd[d]	>1000[d]	0.09 ± 0.02	1×10^{-5}

[a] Co^{2+}-enzyme was prepared as described in Materials and Methods. Co^{2+}-substituted HDAC8 mutants were assayed at 0.1−50 μM HDAC8 with 5−1000 μM substrate at 25 °C in 25 mM Tris, pH 8.0, 140 mM NaCl, and 2.7 mM KCl using a minimum of five substrate concentrations. Initial velocities were determined based on changes in fluorescence. The kinetic parameters and errors were determined from a fit of the Michaelis−Menten equation to the resulting rates using the program Kaleidagraph. [b] Value of k_{cat}/K_M (M^{-1} s^{-1}) relative to Co^{2+}-wild-type HDAC8. [c] Reference *23*. [d] Activity was only detectable above 30 μM enzyme concentrations. At 50 μM enzyme concentrations, the value of k_{cat} could not be determined because the reaction rate increases linearly up to 1 mM substrate when incubated at 25 °C for 1 h. Thus, K_M is greater than 1 mM. [e] Reference *25* reports inactivity; our activity measurements reveal minor residual activity. [f] Catalytic efficiency could not be determined due to lack of detectable activity using up to 10 μM enzyme and 1 mM substrate.

The results of activity measurements for D101A, D101L, D101N, and D101E HDAC8 variants are recorded in Table 2 and are consistent with an important role for this residue in substrate binding. Like D101A HDAC8 (*25*) (Table 2), D101L HDAC8 is catalytically inactive, which is consistent with the necessity for critical enzyme−substrate hydrogen

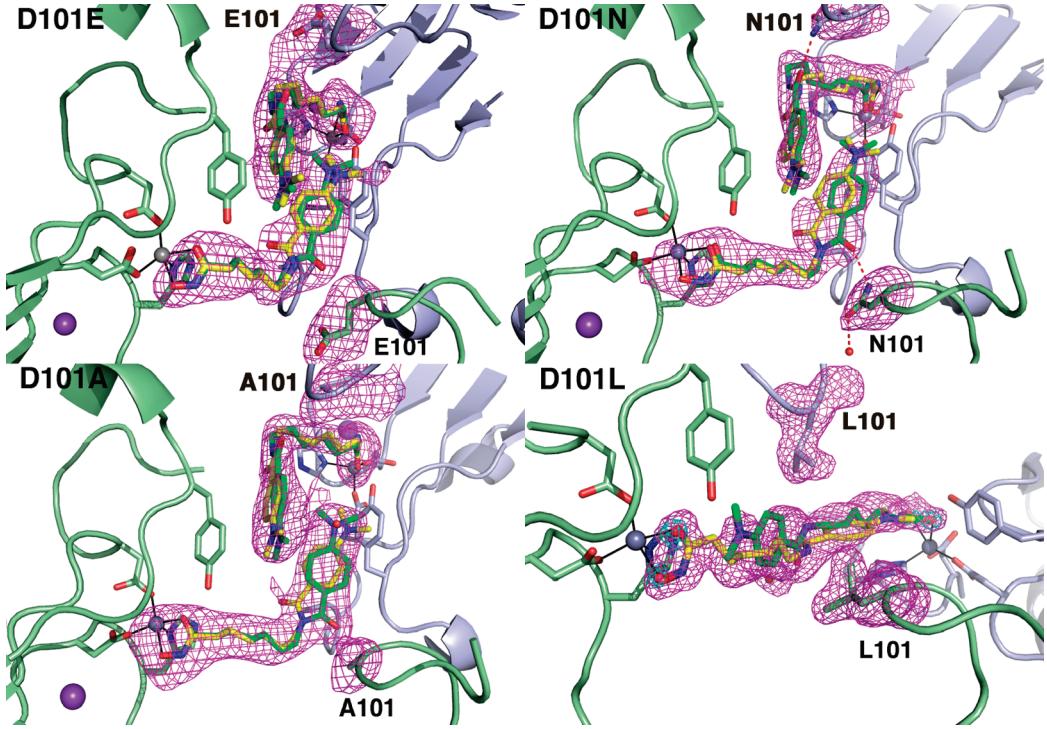

FIGURE 6: Binding of the inhibitor M344 to D101E, D101A, D101N, and D101L HDAC8 variants. The two monomers of the crystallographic dimer are in light green and light blue. Simulated annealing omit maps of inhibitor molecules and residue 101 are superimposed (contoured at 3σ, except for D101A, which is contoured at 2.5σ). Two conformations of the bound inhibitor are observed in the active sites of D101E, D101A, and D101N HDACs (the "yellow" conformation is similar to that observed for binding to the wild-type enzyme). D101L HDAC8 crystallizes in a different space group so the orientation of monomers is different from that observed in the D101E, D101A, and D101N variants. Electron density in the active site of D101L HDAC8 is interpreted as a mixture of 50% bound inhibitor and 50% two zinc-bound solvent molecules that essentially coincide with the positions of the zinc-bound oxygen atoms of the inhibitor (inhibitors bound to each monomer are shown in yellow and green, respectively). Zinc-bound solvent molecules in D101L HDAC8 are shown in cyan and contoured at 6σ. Zinc and potassium ions are in gray and purple, respectively. Zinc coordination interactions are indicated by solid black lines, and hydrogen bonds are indicated by dotted red lines.

bonds involving residue 101. Also consistent with this expectation, the catalytic activity of D101E HDAC8 is only ~7-fold diminished compared to the wild-type enzyme based on the value of k_{cat}/K_M, suggesting that the longer carboxylate side chain of E101 can maintain hydrogen bond acceptor interactions required for substrate binding. Surprisingly, however, D101N HDAC8 exhibits extremely low catalytic activity based on its k_{cat}/K_M and K_M values. Since only the C═O group of the N101 side chain can accept hydrogen bonds, whereas both the Oδ1 and Oδ2 atoms of D101 accept hydrogen bonds from the backbone NH group of the scissile acetyllysine residue and the backbone NH group of the adjacent residue in the $n + 1$ position in the Y306F HDAC8−substrate complex (*25*), the catalytic inactivity of D101N HDAC8 suggests that residue 101 must be a branched hydrogen bond acceptor capable of engaging in two simultaneous hydrogen bond interactions with backbone NH groups of the substrate.

In order to illuminate the structural consequences of D101 amino acid substitutions, we have determined X-ray crystal structures of each HDAC8 variant complexed with the inhibitor M344 (Figure 2), which does not require a hydrogen bond with D101 for binding (*17*). Crystals of the D101A, D101N, and D101E variants grow in the monoclinic space group previously reported for wild-type HDAC8 complexed with a hydroxamate inhibitor (*18*). Crystals of D101L HDAC8 grow in a new orthorhombic crystal form. Increased disorder is seen for the L2 loop in each variant (e.g., the E85−L98 segment is completely disordered), but all D101 variants reveal clear electron density for the L2 loop flanking residue 101.

Inhibitor interactions in the D101 HDAC8 variants complexed with M344 are shown in Figure 6. The inhibitor binding conformation is perturbed in each variant, even though M344 does not directly interact with D101 in the wild-type enzyme (*17*). In complexes with the D101A, D101E, and D101N HDAC8 variants (Figure 6), the inhibitor binds with two alternate conformations for the benzamide ring. The alternate conformer is stabilized by a hydrogen bond interaction with N101 in D101N HDAC8, but E101 is too far (~4 Å) from the inhibitor C═O in the alternate conformer to make a hydrogen bond interaction in D101E HDAC8.

Interestingly, crystal packing in the orthorhombic D101L HDAC8−M344 complex is very different from that observed in the wild-type HDAC8−M344 complex. Electron density for the engineered leucine side chain is clear and unambiguous (Figure 6), and linear electron density is observed between monomer active sites such that inhibitor binding to one monomer is mutually exclusive with inhibitor binding to its symmetry mate. Moreover, inhibitor occupancy is estimated to be ~50%, such that electron density is interpreted for two zinc-bound solvent molecules with 50% occupancy that essentially coincide with the positions of the zinc-bound oxygen atoms of the inhibitor (which does not chelate the Zn^{2+} with favorable geometry). The two zinc-bound solvent molecules exhibit $Zn^{2+}\cdots O$ separations of 2.3 and 2.1 Å. One is within hydrogen-bonding distance to the

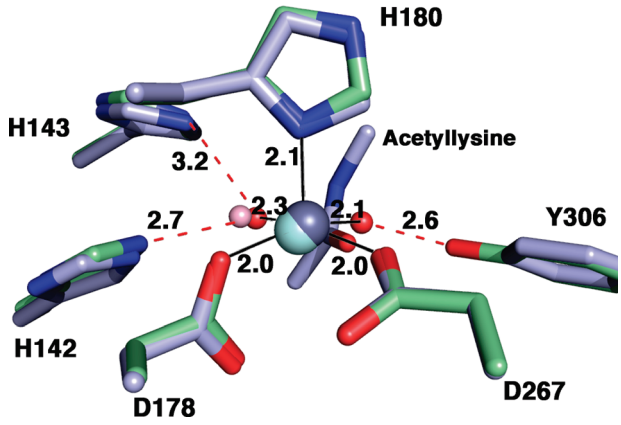

FIGURE 7: Square-pyramidal Zn^{2+} coordination polyhedron in the unliganded form of D101L HDAC8: D178, D267, and two solvent molecules occupy equatorial positions, and H180 occupies the apical position (atoms are color coded as follows: carbon = light green, nitrogen = blue, oxygen = red, Zn^{2+} = gray sphere, H_2O = red spheres). Metal coordination and hydrogen bond interactions are shown in solid black and dotted red lines, respectively. Superimposed are the coordinates of the Y306F HDAC8−substrate complex (PDB accession code 2V5W) (*25*), with atoms color coded similarly except that carbon = light blue, Zn^{2+} = cyan sphere, and H_2O = pink sphere. Note the correspondence of nonprotein coordination sites on zinc.

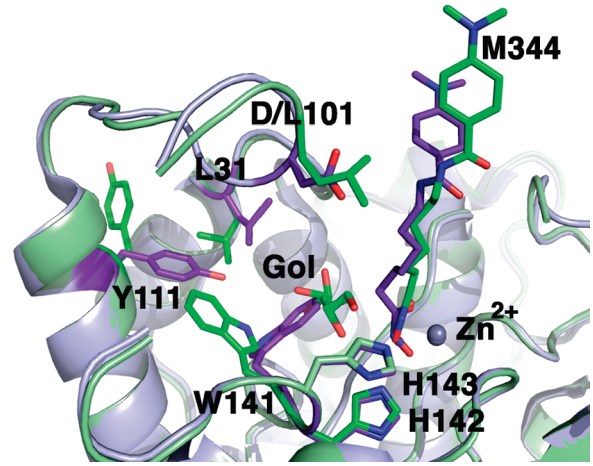

FIGURE 8: Comparison of the wild-type HDAC8−M344 complex (PDB accession code 1T67, light blue protein, purple residues and inhibitor) and the D101L HDAC8−M344 complex (light green protein, green residues and inhibitor) illustrates the "in" and "out" conformations of the aromatic side chains of W141 and Y111. Note that when W141 adopts the "out" conformation, a disordered glycerol molecule (Gol) binds in the resulting void; when Y111 adopts the "out" conformation, the side chain of L31 moves to fill the resulting void.

Y306 hydroxyl group, while the other is within hydrogen-bonding distance to both H142 and H143. Zinc coordination geometry is approximately square pyramidal (Figure 7). One zinc-bound solvent molecule occupies the coordination site previously observed for that of the scissile carbonyl of the substrate complexed with Y306F HDAC8 while the other is in the same location as the zinc-bound solvent molecule in the Y306F HDAC8−substrate complex (*25*).

Unexpectedly, two additional residues, W141 and Y111, exhibit altered conformations in the structures of D101 variants. In the wild-type enzyme complexed with M344, W141 and Y111 are oriented toward the active site Zn^{2+} ion with conformations accordingly designated as "in" (Figure 8). The bulky indole side chain of W141 forms one side of the pocket adjacent to Zn^{2+}, where it makes a van der Waals contact with the acetyllysine substrate (*25*). The side chain of Y111 is adjacent to W141 but closer to the exterior surface of the protein. In the D101L HDAC8−M344 complex, both W141 and Y111 undergo significant conformational changes such that they are oriented away from Zn^{2+}; these are accordingly designated "out" conformations. A disordered molecule of glycerol binds in the resulting void adjacent to Zn^{2+}. In the D101A HDAC8−M344 complex, W141 adopts a predominantly "out" conformation (80% occupancy) with some residual electron density indicative of 20% "in" conformation, and a BME molecule (~50% occupancy) binds in the resulting void adjacent to Zn^{2+}; residue Y111 is characterized by less well defined electron density and modeled to occupy the "in" conformation. In the D101N HDAC8−M344 complex, a slightly disordered W141 adopts a predominantly "out" conformation, and a BME molecule (80% occupancy) binds in the resulting void adjacent to Zn^{2+}; the side chain of Y111 is disordered between the "out" conformation (75% occupancy) and the "in" conformation (25% occupancy). The D101E variant exhibits similar W141 disorder, adopting 60% "out" and 40% "in" conformations with residual density for a BME molecule at 60% occupancy binding similarly to that observed in the N101 and A101 variants; Y111 is disordered with residual density for the "in" conformation. Although the side chain of Y111 is interpreted as disordered in previous crystal structures of HDAC8 (*17, 25*), the only previous observation of an alternate conformation for W141 is in the HDAC8−SAHA complex (*17*). While comparable flexibility is seen for W141 in both the wild-type enzyme (*17*) and E101 variant, even more disorder for W141 is apparent in all catalytically inactive D101 variants. Indeed, in the 1.8 Å resolution structure of the D101L HDAC8−M344 complex, W141 exclusively adopts the "out" conformation. Thus, the catalytic inactivity of D101A, D101N, and D101L HDAC8 variants may not only be due to the loss of important enzyme−substrate hydrogen bonds with D101 but may also be due to alteration of the active site contour resulting from conformational changes of W141.

H143A HDAC8. The H143A substitution abolishes HDAC8 activity (Table 2), so this variant was selected for cocrystallization with a bound substrate molecule. Interestingly, some differences are apparent in substrate binding to this variant as compared to the Y306F HDAC8−substrate complex, which crystallizes in a different space group (*25*). In the structure of the H143A HDAC8−substrate complex, two noncrystallographic dimers are arranged in the asymmetric unit; the interface between these two dimers orders the tetrapeptide substrates in monomers A and C such that their N-terminal acetyl moieties accept hydrogen bonds from the backbone NH groups of K221 in monomers C and A, respectively. The substrates bound to monomers B and D are more disordered at their N-termini. Also, two Zn^{2+} ions (confirmed by anomalous scattering) are observed to cross-link the two dimers in the asymmetric unit, stabilizing the formation of a tetramer. These Zn^{2+} ions are tetrahedrally coordinated by two solvent molecules and a histidine and cysteine from two different monomers: H375 of monomer A and C352 of monomer D coordinate to Zn_A^{2+}; H375 of monomer C and C352 of monomer B coordinate to Zn_B^{2+}.

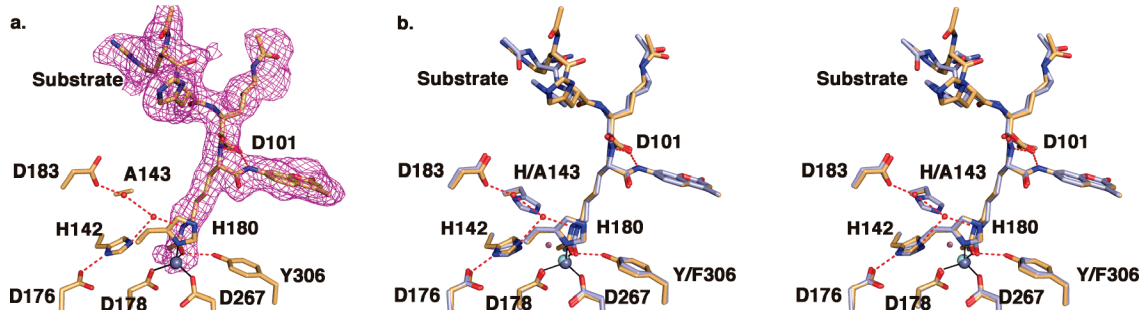

FIGURE 9: (a) Simulated annealing omit map (contoured at 2σ) showing substrate binding to H143A HDAC8. Metal coordination and hydrogen bond interactions are shown as solid black and dotted red lines, respectively. (b) Superposition of the H143A HDAC8−substrate complex (tan) and the previously reported (*25*) Y306F HDAC8−substrate complex (light blue). The zinc ion and water molecules observed in the H143A HDAC8−substrate complex appear as gray and red spheres, respectively. The zinc ion and zinc-bound water molecule observed in the Y306F HDAC8−substrate complex appear as cyan and pink spheres, respectively. Metal coordination and hydrogen bond interactions are shown as solid black and dotted red lines for the H143A HDAC8−substrate complex only.

However, since the buried surface area between Zn^{2+}-linked monomers is less than 5% of the total surface area of each monomer, the observed tetrameric quaternary structure is not biologically significant.

The H143A substitution does not perturb other active site residues, and D101 accepts hydrogen bonds from the backbone NH group of acetyllysine and the backbone NH group of the adjacent residue in the $n + 1$ position of the substrate, as previously observed (*25*). Clear electron density is observed for the carbonyl oxygen of the intact acetyllysine substrate, which coordinates to Zn^{2+} ($Zn^{2+}\cdots O$ separation = 1.9 Å) and accepts a hydrogen bond from Y306 ($O\cdots O$ separation = 2.8 Å) (Figure 9a). In the crystal structure of the Y306F HDAC8−substrate complex, the deletion of the tyrosine hydroxyl group causes the substrate acetyl moiety to shift slightly (~0.5 Å) toward F306. Thus, the current structure is the first to show how both Zn^{2+} and Y306 together can provide simultaneous electrophilic activation of the acetyllysine substrate for nucleophilic attack. However, no electron density is observed for a nucleophilic zinc-bound water molecule, although electron density is observed for two water molecules bridging D183 and the side chain NH group of the acetyllysine substrate in monomers A, B, and C (Figure 9b). This may suggest that the interaction with H143 is important for the positioning or activation of the catalytic water molecule in wild-type HDAC8, which is being further investigated.

CONCLUDING REMARKS

The X-ray crystal structures of HDAC8 and five site-specific variants have been determined in three new crystal forms (one monoclinic and two orthorhombic) in addition to a previously observed monoclinic crystal form (*18*). The polymorphism of HDAC8 crystals appears to be linked to the L1 and L2 loop segments, which also contain residues important for substrate and inhibitor binding. That conformational changes in these loops can be mediated by protein−protein interactions in the crystal lattice may provide a clue as to how protein−protein interactions *in vivo* could regulate HDAC8 function. Moreover, variability in L1 and L2 loop conformations could enable the binding and deacetylation of diverse protein substrates. Structural comparisons of unliganded and liganded HDAC8 reveal that the L2 loop is disordered in the unliganded enzyme but becomes more ordered upon ligand binding to form one wall of the active site as previously hypothesized (*17, 18, 25*). Mutational and structural studies of the only strictly conserved residue in this loop, D101, indicate that residue 101 must be a branched hydrogen bond acceptor capable of engaging in two hydrogen bond interactions with backbone NH groups of the substrate.

The HDAC8 crystal structures additionally illuminate important features regarding the coordination environment and catalytic function of the active site Zn^{2+} ion. The structure of unliganded D101L HDAC8 reveals the presence of two bound solvent molecules that complete an approximately square-pyramidal Zn^{2+} coordination polyhedron (Figure 7). This is reminiscent of the catalytic Zn^{2+} site observed in unliganded LpxC, an unrelated bacterial deacetylase; here, too, two solvent molecules occupy equatorial positions, and a histidine residue occupies the apical position of a square-pyramidal Zn^{2+} coordination polyhedron (*41*). Presumably, the zinc coordination polyhedron in the pre-catalytic Michaelis complex includes both the nucleophilic solvent molecule and the scissile C=O of the substrate, as shown in Figure 1 and as revealed in the crystal structure of Y306F HDAC8 complexed with a tetrapeptide substrate (*25*). Finally, the structure of H143A HDAC8 complexed with an intact acetyllysine tetrapeptide shows how both Zn^{2+} and Y306 can activate the scissile amide carbonyl of the substrate (Figure 9). Future studies will allow us to probe structural changes in the zinc coordination polyhedron that are required for catalysis.

REFERENCES

1. Gilbert, N., and Ramsahoye, B. (2005) The relationship between chromatin structure and transcriptional activity in mammalian genomes. *Briefings Funct. Genomics Proteomics 4*, 129–142.
2. Holbert, M. A., and Marmorstein, R. (2005) Structure and activity of enzymes that remove histone modifications. *Curr. Opin. Struct. Biol. 15*, 673–680.
3. Vaquero, A., Loyola, A., and Reinberg, D. (2003) The constantly changing face of chromatin. *Sci. Aging Knowledge Environ. 2003*, RE4.
4. Cosgrove, M. S., and Wolberger, C. (2005) How does the histone code work? *Biochem. Cell Biol. 83*, 468–476.
5. Eberharter, A., and Becker, P. B. (2002) Histone acetylation: a switch between repressive and permissive chromatin. Second in review series on chromatin dynamics. *EMBO Rep. 3*, 224–229.
6. Eberharter, A., Ferreira, R., and Becker, P. (2005) Dynamic chromatin: concerted nucleosome remodelling and acetylation. *Biol. Chem. 386*, 745–751.

7. Kuo, M. H., and Allis, C. D. (1998) Roles of histone acetyltransferases and deacetylases in gene regulation. *BioEssays 20*, 615–626.
8. Thiagalingam, S., Cheng, K. H., Lee, H. J., Mineva, N., Thiagalingam, A., and Ponte, J. F. (2003) Histone deacetylases: unique players in shaping the epigenetic histone code. *Ann. N.Y. Acad. Sci. 983*, 84–100.
9. Marmorstein, R. (2001) Structure of histone deacetylases: insights into substrate recognition and catalysis. *Structure 9*, 1127–1133.
10. Gregoretti, I. V., Lee, Y. M., and Goodson, H. V. (2004) Molecular evolution of the histone deacetylase family: functional implications of phylogenetic analysis. *J. Mol. Biol. 338*, 17–31.
11. de Ruijter, A. J., van Gennip, A. H., Caron, H. N., Kemp, S., and van Kuilenburg, A. B. (2003) Histone deacetylases (HDACs): characterization of the classical HDAC family. *Biochem. J. 370*, 737–749.
12. Lin, H. Y., Chen, C. S., Lin, S. P., Weng, J. R., and Chen, C. S. (2006) Targeting histone deacetylase in cancer therapy. *Med. Res. Rev. 26*, 397–413.
13. Hu, E., Chen, Z., Fredrickson, T., Zhu, Y., Kirkpatrick, R., Zhang, G. F., Johanson, K., Sung, C. M., Liu, R., and Winkler, J. (2000) Cloning and characterization of a novel human class I histone deacetylase that functions as a transcription repressor. *J. Biol. Chem. 275*, 15254–15264.
14. Lee, H., Sengupta, N., Villagra, A., Rezai-Zadeh, N., and Seto, E. (2006) Histone deacetylase 8 safeguards the human ever-shorter telomeres 1B (hEST1B) protein from ubiquitin-mediated degradation. *Mol. Cell. Biol. 26*, 5259–5269.
15. Waltregny, D., Glenisson, W., Tran, S. L., North, B. J., Verdin, E., Colige, A., and Castronovo, V. (2005) Histone deacetylase HDAC8 associates with smooth muscle alpha-actin and is essential for smooth muscle cell contractility. *FASEB J. 19*, 966–968.
16. Balasubramanian, S., Ramos, J., Luo, W., Sirisawad, M., Verner, E., and Buggy, J. J. (2008) A novel histone deacetylase 8 (HDAC8)-specific inhibitor PCI-34051 induces apoptosis in T-cell lymphomas. *Leukemia 22*, 1026–1034.
17. Somoza, J. R., Skene, R. J., Katz, B. A., Mol, C., Ho, J. D., Jennings, A. J., Luong, C., Arvai, A., Buggy, J. J., Chi, E., Tang, J., Sang, B. C., Verner, E., Wynands, R., Leahy, E. M., Dougan, D. R., Snell, G., Navre, M., Knuth, M. W., Swanson, R. V., McRee, D. E., and Tari, L. W. (2004) Structural snapshots of human HDAC8 provide insights into the class I histone deacetylases. *Structure 12*, 1325–1334.
18. Vannini, A., Volpari, C., Filocamo, G., Casavola, E. C., Brunetti, M., Renzoni, D., Chakravarty, P., Paolini, C., De Francesco, R., Gallinari, P., Steinkuhler, C., and Di Marco, S. (2004) Crystal structure of a eukaryotic zinc-dependent histone deacetylase, human HDAC8, complexed with a hydroxamic acid inhibitor. *Proc. Natl. Acad. Sci. U.S.A. 101*, 15064–15069.
19. Finnin, M. S., Donigian, J. R., Cohen, A., Richon, V. M., Rifkind, R. A., Marks, P. A., Breslow, R., and Pavletich, N. P. (1999) Structures of a histone deacetylase homologue bound to the TSA and SAHA inhibitors. *Nature 401*, 188–193.
20. Kanyo, Z. F., Scolnick, L. R., Ash, D. E., and Christianson, D. W. (1996) Structure of a unique binuclear manganese cluster in arginase. *Nature 383*, 554–557.
21. Colleluori, D. M., Reczkowski, R. S., Emig, F. A., Cama, E., Cox, J. D., Scolnick, L. R., Compher, K., Jude, K., Han, S., Viola, R. E., Christianson, D. W., and Ash, D. E. (2005) Probing the role of the hyper-reactive histidine residue of arginase. *Arch. Biochem. Biophys. 444*, 15–26.
22. Dowling, D. P., Di Costanzo, L., Gennadios, H. A., and Christianson, D. W. (2008) Evolution of the arginase fold and functional diversity. *Cell. Mol. Life Sci. 65*, 2039–2055.
23. Gantt, S. L., Gattis, S. G., and Fierke, C. A. (2006) Catalytic activity and inhibition of human histone deacetylase 8 is dependent on the identity of the active site metal ion. *Biochemistry 45*, 6170–6178.
24. Gantt, S. L. (2006) Ph.D. Dissertation, University of Michigan.
25. Vannini, A., Volpari, C., Gallinari, P., Jones, P., Mattu, M., Carfi, A., De Francesco, R., Steinkuhler, C., and Di Marco, S. (2007) Substrate binding to histone deacetylases as shown by the crystal structure of the HDAC8-substrate complex. *EMBO Rep. 8*, 879–884.
26. Schuetz, A., Min, J., Allali-Hassani, A., Loppnau, P., Kwiatkowski, N. P., Mazitschek, R., Edwards, A. M., Arrowsmith, C. H., Vedadi, M., Bochkarev, A. and Plotnikov, A. N. (2008) Crystal structure of the human histone deacetylase HDAC7 (DOI 10.2210/pdb3c0y/pdb).
27. Nielsen, T. K., Hildmann, C., Dickmanns, A., Schwienhorst, A., and Ficner, R. (2005) Crystal structure of a bacterial class 2 histone deacetylase homologue. *J. Mol. Biol. 354*, 107–120.
28. Otwinowski, Z., and Minor, W. (1997) Processing of X-ray diffraction data collected in oscillation mode. *Methods Enzymol. 276*, 307–326.
29. Leslie, A. G. W. (1992) *Crystallographic computing V: from chemistry to biology*, Oxford University Press, New York.
30. Navaza, J. (1994) AMoRe: an automated package for molecular replacement. *Acta Crystallogr. A 50*, 157–163.
31. McCoy, A. J., Grosse-Kunstleve, R. W., Adams, P. D., Winn, M. D., Storoni, L. C., and Read, R. J. (2007) Phaser crystallographic software. *J. Appl. Crystallogr. 40*, 658–674.
32. Brünger, A. T., Adams, P. D., Clore, G. M., De Lano, W. L., Gros, P., Grosse-Kunstleve, R. W., Jiang, J. S., Kuszewski, J., Nilges, M., Pannu, N. S., Read, R. J., Rice, L. M., Simonson, T., and Warren, G. L. (1998) Crystallography & NMR system: a new software suite for macromolecular structure determination. *Acta Crystallogr. D 54*, 905–921.
33. Jones, T. A., Zou, J. Y., Cowan, S. W., and Kjeldjaard, M. (1991) Improved methods for building protein models in electron density maps and the location of errors in these models. *Acta Crystallogr. A 47*, 110–119.
34. Schultz, B. E., Misialek, S., Wu, J., Tang, J., Conn, M. T., Tahilramani, R., and Wong, L. (2004) Kinetics and comparative reactivity of human class I and class IIb histone deacetylases. *Biochemistry 43*, 11083–11091.
35. Mai, A., Massa, S., Ragno, R., Cerbara, I., Jesacher, F., Loidl, P., and Brosch, G. (2003) 3-(4-Aroyl-1-methyl-1*H*-2-pyrrolyl)-*N*-hydroxy-2-alkylamides as a new class of synthetic histone deacetylase inhibitors. 1. Design, synthesis, biological evaluation, and binding mode studies performed through three different docking procedures. *J. Med. Chem. 46*, 512–524.
36. Hildmann, C., Wegener, D., Riester, D., Hempel, R., Schober, A., Merana, J., Giurato, L., Guccione, S., Nielsen, T. K., Ficner, R., and Schwienhorst, A. (2006) Substrate and inhibitor specificity of class 1 and class 2 histone deacetylases. *J. Biotechnol. 124*, 258–270.
37. Matthews, B. W. (1988) Structural basis of the action of thermolysin and related zinc peptidases. *Acc. Chem. Res. 21*, 333–340.
38. Christianson, D. W., and Lipscomb, W. N. (1989) Carboxypeptidase A. *Acc. Chem. Res. 22*, 62–69.
39. Bottomley, M. J., Lo Surdo, P., Di Giovine, P., Cirillo, A., Scarpelli, R., Ferrigno, F., Jones, P., Neddermann, P., De Francesco, R., Steinkuhler, C., Gallinari, P., and Carfi, A. (2008) Structural and functional analysis of the human HDAC4 catalytic domain reveals a regulatory structural zinc-binding domain. *J. Biol. Chem. 283*, 26694–26704.
40. Schafer, S., Saunders, L., Eliseeva, E., Velena, A., Jung, M., Schwienhorst, A., Strasser, A., Dickmanns, A., Ficner, R., Schlimme, S., Sippl, W., Verdin, E., and Jung, M. (2008) Phenylalanine-containing hydroxamic acids as selective inhibitors of class IIb histone deacetylases (HDACs). *Bioorg. Med. Chem. 16*, 2011–2033.
41. Gennadios, H. A., Whittington, D. A., Li, X., Fierke, C. A., and Christianson, D. W. (2006) Mechanistic inferences from the binding of ligands to LpxC, a metal-dependent deacetylase. *Biochemistry 45*, 7940–7948.

BI801610C